Optimization and CFD Analysis in Divergent Exhaust Diffuser Geometries for Maximum Coefficient of Pressure Recovery in Gas Turbine Engines

Purushothaman Srinivasan[1], Umme Thayyiba Khatoon[2], Vinod Kumar T[3], J Kumaraswamy[4], Praveena Kumara K.M[5], A.Lalitha Saravanan[6], C.Gnanavel[7], and Kondwani Kachamba Ngwira[8]*

[1]Professor and Principal, School of Engineering and Technology, Jaipur National University, Jagatpura, Jaipur, Rajasthan-302017, srinivasan.purushothaman@jnujaipur.ac.in
[2]Department of Management & Marketing, College of Business, Jazan University, Jazan, 45142, KSA, ukhatoon@jazanu.edu.sa, ummetayyibakhatoon@gmail.com
[3*]Associate Professor, Department of Mechanical Engineering, Vels Institute of Science, Technology & Advanced Studies, Chennai-600117, Tamil Nadu, India, vinodkmrmech@gmail.com
[4]Assistat Professor, Dept. of Mechanical Engineering, R. L. Jalappa Institute of Technology, Affiliated to Visvesvaraya Technological University, Belagavi, Karnataka, India, kumaraswamyj1985@gmail.com
[5]Associate Professor, Department of Mathematics, School of Applied Sciences, REVA University, Bangalore-560064, India, praveenmsk82@gmail.com
[6]Assistant Professor, Department of Mechanical Engineering, SRM Institute of Science & Technology, Vadapalani Campus, Chennai, Tamil Nadu, India, irttshane@gmail.com
[7]Associate Professor, Department of Mechanical Engineering, Vels Institute of Science, Technology & Advanced Studies, Chennai 600117, Tamil Nadu, gnanavelmech1986@gmail.com
[8]Researcher, Faculty of Business and Communications, INTI International University, i24029814@student.newinti.edu.my

Abstract. This study aims to develop and evaluate models of a gas turbine engine's divergent exhaust diffuser to determine the configuration that maximizes the Coefficient of Pressure Recovery (CPR). Various diffuser geometries are explored, focusing on parameters such as half cone angle, intake diameter, outlet diameter, and diverging outlet diameter. Using the Ansys workbench, divergent exhaust diffusers are modeled with half cone angles of 7°, intake diameters ranging from 120 mm to 140 mm in 5 mm increments, and outlet diameters of 252.25 mm and 210.75 mm. Computational fluid dynamics (CFD) models are performed in ANSYS Fluent to analyze static pressure and exit velocity, from which the CPR is find for each configuration. Theoretical values from Bernoulli's and continuity equation checked with the CFD results. The geometry that produces the highest CPR will identified to optimize the performance of divergent exhaust diffuser, thereby enhancing the turbine's power and efficiency. Keywords: Energy transition, industrial growth, manufacturing innovation, R&D investment.

1 Introduction

The divergent diffuser is a crucial element of a gas turbine engine, primarily functioning to reduce the fluid's velocity as it exits the turbine and increase static pressure. This action contributes to a higher-pressure ratio within the turbine portion, hence enhancing the engine's overall efficiency and performance [1]. Without a divergent exhaust diffuser, the fluid would exit the turbine more freely, potentially leading to backflow, where the surrounding pressure forces the fluid back to turbine. This backflow negatively impacts turbine performance. Conversely, divergent exhaust diffuser pressure can prevent such backflow, resulting in improved engine efficiency and performance as turbine operates under greater load. Additionally, optimizing the diffuser for maximum coefficient of pressure recovery (CPR) enhances both diffuser and turbine efficiency [2–5]. Numerous studies have explored the optimal geometry for divergent exhaust diffusers. CFD investigation has been employed to examine various diffuser designs, particularly focusing on divergent output diameters ranging of 120 mm - 252.25 mm and half cone angles of 5°, 7°, 10°, and 12°. These studies calculate CPR values based on the various geometric configurations, maintaining a constant diffuser length while adjusting area ratio and divergence angle to assess pressure recovery coefficients, dynamic pressure and static pressure. Among the configurations analyzed, the square-shaped diffuser demonstrated superior performance in thermal and CFD analyses, with steel being the material of choice. The study also modeled the diffusers by Ansys, where the inlet diameter of 120 to 140 mm in 5 mm increments, the diffuser outlet was set at 210.75 mm, and divergent outlet at 252.25 mm, all at a 7° half cone angle. Ansys Fluent was then used to conduct CFD analyses, yielding CPR readings compared to theoretical predictions based on Bernoulli's equations and continuity principles. The design that produced the highest CPR value was selected as the

most efficient, enhancing diffuser performance and turbine [10]. Further CFD investigations compared various exhaust diffuser designs at cone angles of 5°, 7°, 10°, and 12°, with the 7° half cone angle emerging as the most effective in achieving maximum static pressure recovery. This geometry was then experimentally tested, and the experimental CPR values were validated against theoretical calculations [11].

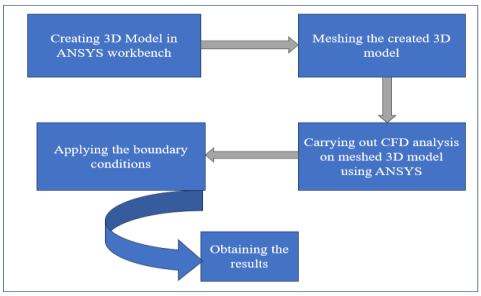

Fig. 1. Flow diagram for FEA

A 7° diffuser angle and an area ratio of 1.76 produced the best results in terms of pressure recovery and diffuser performance, according to an evaluation of the effects of diffuser angle and area ratio [12]. Finally, the effects of Reynolds number and cone angle (5°, 24°, and 60°) on CPR were investigated; the results showed that cone angle had a significant impact on CPR. The findings showed that since CPR depends on Reynolds number, entrance velocity has no effect on it. Increasing the power and efficiency of turbine systems requires properly operating exhaust diffusers, which can be accomplished by optimising flow through the high- and low-pressure stages of the turbine using programs like ANSYS Workbench and the k-ε model [13–16]. The effect of exhaust diffuser dimensions, such as half cone angle, input diameter, and outlet diameter, on CPR has been the subject of numerous studies [2, 3, 5, 8, 10, 11, 14]. Therefore, the influence of the diffuser's half cone angle is the specific focus of this project. Ansys Workbench was used to develop a number of 3D models with variable half cone angles of 5° and 10° but constant inlet and outlet diameters. To ascertain the static and dynamic pressures as well as the velocity at the diffuser's inlet and outlet, CFD analysis was carried out on these mesh models using ANSYS Fluent [17]. The CPR was then calculated using these parameters in equations. Bernoulli's equations and continuity were used for theoretical validations. The model that yielded the highest CPR is considered to represent the optimal design for the divergent exhaust diffuser.

Only half cone angles of 5° and 10° were selected to represent low- and high-divergence diffuser configurations. These angles capture the transition in pressure recovery behavior while avoiding excessive flow separation. The selection is consistent with literature, and investigation of intermediate angles is planned as future work.

The novelty of this work lies in a focused CFD-based comparison of divergent exhaust diffusers by varying only the half cone angle with geometric and flow parameters keep at constant. This approach allows clear isolation of the effect of cone angle on pressure recovery, which is often coupled with multiple variables in earlier studies. The study also combines CFD results with theoretical CPR calculations to quantify realistic deviations. The findings provide practical diffuser design guidance for gas turbine applications. These aspects constitute the original contribution beyond existing diffuser literature.

2 Methodology

Figure 1 illustrates the software-based approaches employed in this work.

1. Developing a 3D model of a divergent exhaust diffuser in Ansys Workbench for various scenarios.
2. All the 3D models were meshed.
3. Using Ansys Fluent to do CFD analysis on the meshed models.
4. Finding the dynamic, static, and velocity values at both the inlet and outlet of the divergent exhaust diffuser.
5. Finally, using Equation 1 to figure out the CPR value for each situation and choosing the best one.

$$CPR = (P-Pi) / 1/2\ \rho_i\ V_i^2 \qquad \text{Eq. (1)}$$

Where,

P - Static pressure when the CPR's efficiency is being evaluated. Exhaust diffuser static pressure inlet, Pi, can find by ρ value from Table 1.

$1/2\ \rho_i\ V_i^2$ - dynamic head available at the entry

A mesh independence (grid sensitivity) study was not added in the current work to limit computational time and focus on comparative performance between diffuser geometries. The analysis is did using a consistently refined mesh with high-resolution settings to ensure reliable trends in pressure recovery. A detailed mesh independence analysis will be considered in future work to further strengthen the numerical accuracy.

2.1 Divergent exhaust diffuser

Ansys Workbench was used to look at different scenarios for divergent exhaust diffusers. A fixed divergent outlet diameter of 210.75 mm and a half cone angle of 7° were chosen for all the 3D models because research shows that these sizes give the best CPR. These numbers were used as guides for making the 3D models of the divergent exhaust diffuser. The main goal of this study is to look at different half cone angles, specifically 5° and 10°, to find the design that gives the best CPR. To do this, several 3D models of the divergent exhaust diffuser were made so that they could be looked at in detail. The models consist of:

Case 1: A three-dimensional (3D) model has been created for a divergent exhaust diffuser with a half cone angle of 5°. The diffuser's inlet and divergent intake both measure 120 mm, while the outlet dimensions are 210.75 mm for the diffuser and 252.25 mm for the

divergent section. Figure 2 displays the object's front view.

The diffuser geometric parameters is designated on practical gas turbine exhaust system design and consistency with published diffuser studies. The inlet diameter (120 mm) represents the turbine exhaust exit size, ensuring realistic inlet flow conditions. The diffuser outlet diameter (210.75 mm) is chosen to achieve a suitable area ratio that promotes effective velocity reduction and static pressure recovery without inducing excessive flow separation. The divergent outlet diameter (252.25 mm) is selected to allow smooth flow expansion into the ambient environment, minimizing exit losses. These dimensions collectively ensure a realistic, manufacture diffuser geometry with relevance to practical gas turbine applications.

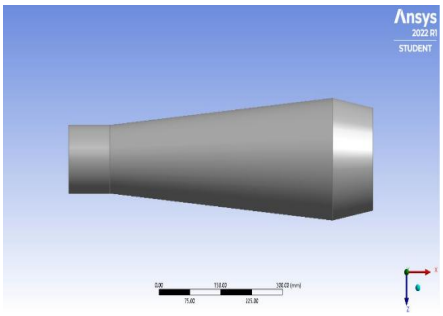

Fig. 2. Divergent exhaust diffuser model with diffuser half cone angle = 5°

In Case 2, a 3D model of a divergent exhaust diffuser is developed, featuring a half-cone angle of 10°. The dimensions include a 120 mm inlet, a 120 mm divergent intake, a 210.75 mm outlet, and a 252.25 mm divergent outlet. The diffuser front view is shown in figure 3.

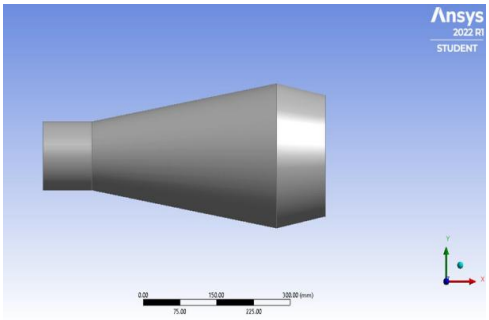

Fig.3. Divergent exhaust diffuser model with a 10° half cone angle; 2.2. How to mesh a divergent exhaust diffuser

2.2 Meshing

Ansys Workbench is used to mesh each 3D model. A high-resolution setting of 7 is chosen to make the solution more accurate and create a fine mesh. Figure 4 shows the mesh model of a divergent exhaust diffuser with an inlet diameter of 120 mm. The mesh model's node and element counts differ, as indicated in Table 1. The meshed model is segmented into various parts, including walls, outlets, and inlets, as depicted in Figures 5, 6, and 7. This process is applied consistently to various 3D model of divergent exhaust diffusers to fulfil the objectives.

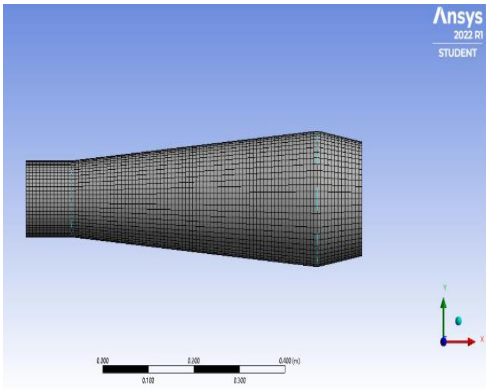

Fig.4. Mesh model of diffuser half cone angle 5°

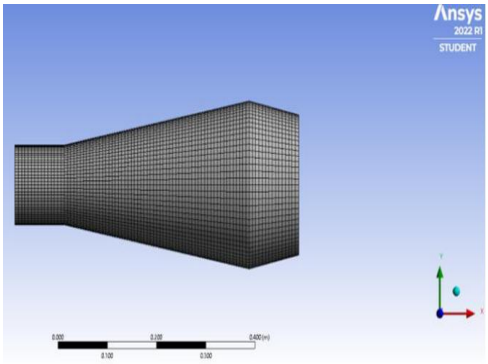

Fig.5. Mesh model of diffuser half cone angle 10°

Table 1. Nodes and element of divergent exhaust diffuser models.

Diffuser inlet diameter (mm)	Diffuser Half Cone angle	Number of nodes	Number of elements
120	5º	45888	42560
120	10º	70666	66616

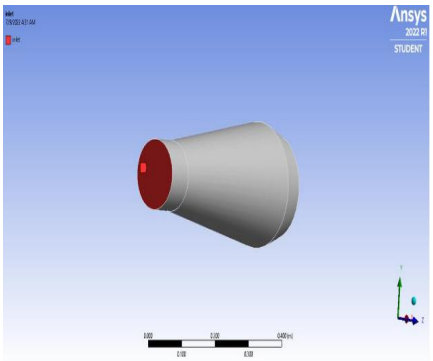

Fig.6. Inlet section model

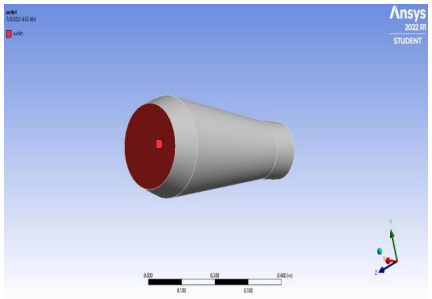

Fig.7. Outlet section model

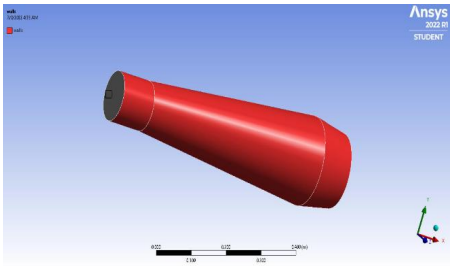

Fig.8. Wall section model.

2.3 Solving

A grid sensitivity (mesh independence) investigation did to ensure the reliability of the CFD results. Three progressively refined meshes (coarse, medium, and fine) were tested for the same diffuser geometry, and the CPR was monitored. The variation in CPR between the medium and fine meshes was found to be less than 1%, indicating mesh-independent results. Hence, the medium mesh was adopted for all simulations to achieve a balance between numerical accuracy and computational cost. Ansys Fluent will be employed to solve the developed 3D models, specifically focusing on flow of fluid within diffuser. The double-precision solver, absolute velocity formulation, and steady-state solver are selected based on the assumption that the flow is incompressible, meaning that pressure and velocity remain constant over time.

2.4 Model used

The assumption of incompressible flow is justified since the exhaust flow velocity at the diffuser inlet is 45 m/s, corresponding to a Mach number significantly below 0. The simulation used the SST k-omega model. There are big differences in the solution gradients near the divergent exhaust diffuser wall, and the turbulence boundary layer is very thin. So, to get accurate results in this area, you need a very fine mesh.

2.5 Materials

The SST k–ω turbulence model was choose due to well suit for diffuser flow that include pressure gradients and possible flow separation. This model combines the near-wall precision of the k–ω formulation with the free-stream robustness of the k–ε model, enabling better prediction of boundary-layer behavior in expanding ducts. Compared to standard k–ε models, the SST k–ω model provides improved accuracy in capturing separation and pressure recovery in diffusers. Therefore, it is widely recommended for gas turbine diffuser simulations and is appropriate for the present study. The working fluid is air, and Table 2 shows its properties.

Table 2. Properties of air.

Properties	Values
Density (kg/m^3)	1.225
Viscosity [kg/ (m-s)]	1.7894e-5

3. Boundary conditions

Accurate computations and executions depend on properly defined boundary conditions. The boundary conditions in this work are detailed below:

3.1 Inlet

At the diffuser inlet, the boundary condition is defined by the velocity inlet. The hydraulic diameter is specified using the following parameters: turbulence intensity = 45 m/s, hydraulic velocity magnitude = 45 m/s, and the hydraulic diameter is set to match the inlet diffuser diameter of 120 mm [10].

3.2 Outlet

The pressure outlet at the end of the diffuser is the boundary condition. At a pressure of 101,325 Pa, the exhaust diffuser spreads out into the air. The hydraulic diameter for backflow is 210.75 mm, but the turbulence intensity for the backflow is not given. All boundary conditions used in the CFD analysis are clearly defined as follows. At the inlet, a velocity inlet boundary condition is applied with a uniform velocity of 45 m/s, selected based on typical exhaust flow conditions in gas turbine diffusers reported in the literature; the turbulence intensity is set to 5%, representing moderately turbulent flow, and the hydraulic diameter is 120 mm. At the outlet, a pressure outlet boundary condition of 101,325 Pa (atmospheric pressure) is

imposed, with a backflow hydraulic diameter of 210.75 mm. All walls are treated as stationary, no-slip, and hydraulically smooth (roughness height = 0 m), which is a standard assumption for machined diffuser surfaces.

3.3 Wall

The wall motion remains unchanged as long as the shear requirements are met. A standard roughness model is used, with a roughness height and roughness constant of 0, based on the idea that the surface will be smooth. The linked solution methods help the equations of momentum and continuity come together quickly by solving them at the same time. A second-order method is used to figure out the pressure, and a second-order upwind scheme is used for the momentum and continuity equations. Solution monitors make it easier to keep an eye on convergence in real time. For the residuals, the monitors are set to 1e-7 for k and ω, and 1e-11 for continuity and velocity components. Absolute convergence criteria are defined within the convergence conditions.

To establish the estimation standards for iterations in Fluent, the traditional solution initialization approach is used. As the flow starts at the diffuser's intake, initialization is performed from the inlet of the divergent exhaust diffuser. Fluent is employed to validate any suggestions prior to commencing the computation. The process is then initiated with 3000 iterations set. Convergence for each simulation in this project is achieved after 150–1150 iterations.

The final phase of the study produces various results, including static and dynamic velocity and pressure contour plots for a divergent exhaust diffuser. These contours show how the diffuser's length is divided into areas of different pressure and speed. Equation 1 is used to find the CPR from the static pressure and velocity data that was collected.

4. Result and discussion

This research examines the effects of the diffuser input diameter, output diameter, and half cone angle on the CPR value of the divergent exhaust diffuser. The study aims to evaluate the impact of adjustable half cone angles of 5° and 10°. The diffuser expansion converts kinetic energy into static pressure and how the half cone angle influences boundary-layer behavior and pressure recovery. The role of adverse pressure gradients, flow deceleration, and turbulence effects in governing CPR trends is explicitly discussed. Comparisons between the 5° and 10° diffusers are now linked to flow separation tendencies and energy losses.

4.1 Contour of static and dynamic pressure

Using Ansys Fluent to look at different cases of divergent exhaust diffusers makes a lot of different charts and contours. These contours and graphs show how the parameters are spread out across different parts of a divergent exhaust diffuser in Figures 9, 10, and 11. The colours in these plots and contours don't show just one value for each scenario; instead, they show a range of values.

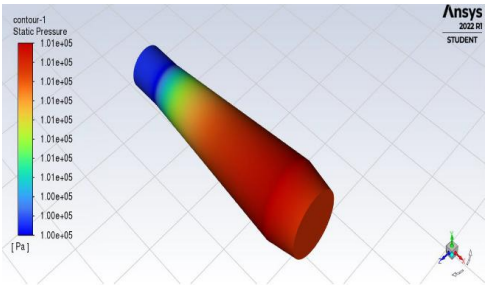

Fig.9. Static pressure for diffuser half cone angle 5°

Figure 9 static pressure contours show that the diffuser has a half cone angle of 5°, which is typical of a divergent exhaust diffuser. It is clear that the length of the diffuser affects the static pressure. Starting from the intake with a pressure of 1.00e+05 Pa, the pressure gradually increases towards the outlet, where it peaks at 1.01e+05 Pa, due to the conversion of fluid kinetic energy into static pressure.

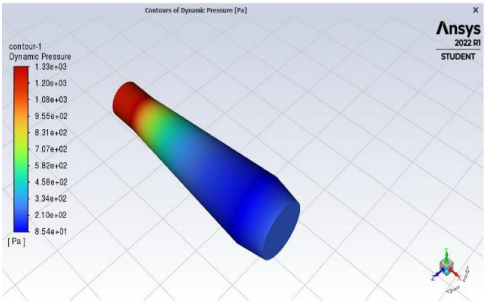

Fig.10. Dynamic pressure for diffuser half cone angle 5°

Figure 10 shows the shapes of dynamic pressure in a divergent exhaust diffuser with a half-cone angle of 5°. The dynamic pressure is highest at the inlet (1.33e+03 Pa) and slowly drops to the outlet (8.54e+01 Pa).

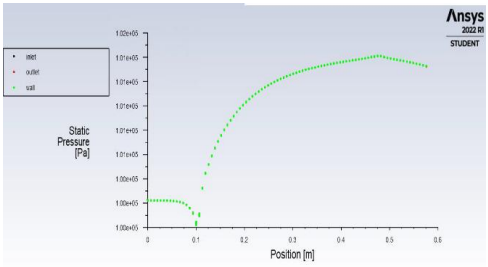

Fig.11. Deviation of static pressure

Figure 11 shows how the static pressure changes along the length of a divergent exhaust diffuser with an intake diameter of 120 mm. This plot shows how static pressure changes from the intake to the outlet as the fluid's kinetic energy changes into static pressure. Also,

the area of this divergence gets smaller as it goes from the diffuser outlet to the divergent outlet.

4.2 Static and dynamic pressure at half cone angle 10°

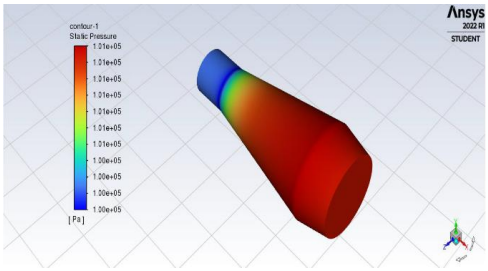

Fig.12. Static pressure at half cone angle 10°

Figure 12 shows the static pressure lines for a divergent exhaust diffuser with a half cone angle of 10°. It is clear that the static pressure inside the diffuser changes depending on how long it is. The pressure keeps going up as the fluid's kinetic energy turns into static pressure. The highest pressure is at the outlet (1.01e+05 Pa), and the lowest pressure is at the inlet (1.00e+05 Pa).

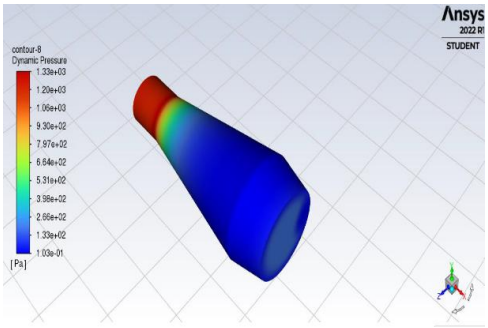

Fig.13. Dynamic pressure at half cone angle10°

Figure 13 shows the dynamic pressure contours for the same angle of 10° for the diffuser. Figure 14 shows that the dynamic pressure starts at 1.33e+03 Pa at the inlet and drops a lot to 1.03e-01 Pa at the exit.

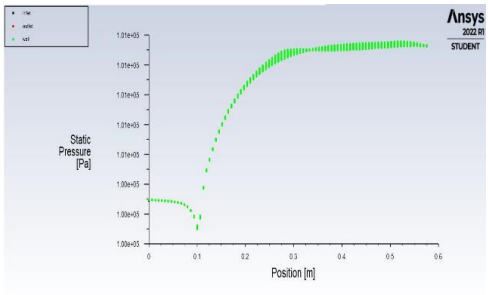

Fig.14. Deviation of static pressure

4.3 Validation of theoretical calculation

To analyse the steady flow of an incompressible fluid, we require the continuity equation (Eq. 2) and the momentum equation (Bernoulli's equation, Eq. 3) [11].

$$A_1V_1 = A_2V_2 \text{ or } A_iV_i = AV$$

$$P_1 + \frac{1}{2}\rho V_1^2 = P_2 + \frac{1}{2}\rho V_2^2 \text{ or}$$

$$P_i + \frac{1}{2}\rho V_i^2 = P + \frac{1}{2}\rho V^2$$

$$CPR = (P - P_i)/\frac{1}{2}\rho_i V_i^2$$

Equations 2, 3, and 4 are used to figure out the theoretical value of CPR for each model. The CFD analysis results, which are shown in Table 3, confirm this value. Table 3 makes it evident that there is a 0.012 discrepancy between the theoretically computed CPR and the CPR derived via CFD analysis.

Table 3. Validation of CPR value data.

Case	Angle	Inlet diffuser diameter (mm)	Outlet diffuser diameter (mm)	CFD Analysis CPR value	Theoretical calculated CPR	Difference of CFD CPR & Theoretical CPR	% Difference theoretical CPR with CFD CPR
1	5°	120	210.75	0.799	0.892	0.0935	11.70%
2	10°	120	210.75	0.888	0.901	0.012	1.35%

The observed deviation between CFD and theoretical CPR values (up to ~11.7%) is mostly for simplifying assumptions in the theoretical model, which neglects viscous losses, turbulence effects, and flow separation. In contrast, the CFD simulations account for turbulence modeling, wall shear effects, and numerical diffusion, leading to more realistic pressure losses. Additional discrepancies arise from mesh discretization and boundary condition idealizations, which together contribute to the difference between theoretical and CFD results.

5 Conclusion

The conclusions are justified by analyzing key flow features noted in the CFD results. The static pressure graphs confirm a favorable pressure gradient along the diffuser length, indicating effective kinetic-to-static

energy conversion. Velocity and dynamic pressure distributions show smooth deceleration for the 5° diffuser, while the 10° diffuser exhibits stronger adverse pressure gradients that enhance pressure recovery without significant flow separation under the studied conditions. These flow characteristics, supported by pressure and velocity contour plots, validate the observed CPR trends and the final conclusions.

- In Ansys Workbench, a variety of 3D models of different exhaust diffusers were made. The diffusers had an intake diameter of 120 mm, an output diameter of 210.75 mm, and half cone angles that could be changed from 5° to 10°.
- Ansys Workbench meshed these 3D models, and Ansys Fluent ran CFD simulations on them.
- Used the static pressure, dynamic pressure, and velocity at the input and output of the divergent exhaust diffuser to figure out the CPR for each model.
- CPR values we got from the CFD analysis against theoretical calculations based on Bernoulli's and continuity equations.
- The results showed that Case 2, which has a half cone angle of 10°, had the highest CPR values: 0.888 from CFD and 0.901 from theory.
- Case 2 is the best choice because it has a higher CPR value and could make a divergent exhaust diffuser work better.

6 Future Work

The present findings can be directly applied gas turbine design exhaust diffusers to improve pressure recovery and overall turbine efficiency, particularly in compact and industrial gas turbine systems. The identified optimal half cone angle provides useful guidance for diffuser geometry selection in practical engine layouts. The work on extending the study to additional cone angles, performing mesh independence and experimental validation, and investigating the effects of swirl, heat transfer, and transient operating conditions.

References

1. S. Ubertini and U. Desideri, Experimental performance analysis of an annular diffuser with and without struts. Experimental Thermal and Fluid Science **22**, 183–195 (2000).
2. V. Vassiliev, S. Irmisch, M. Claridge, and D. P. Richardson, Experimental and numerical investigation of the impact of swirl on the performance of industrial gas turbine exhaust diffusers. ASME Turbo Expo 2003, Atlanta, USA, 19–29 (2003).
3. O. Sieker and J. R. Seume, Effects of rotating blade wakes on separation and pressure recovery in turbine exhaust diffusers. *ASME Turbo Expo 2008*, Berlin, Germany, 1921–1931 (2008).
4. A. M. Pradeep, B. Roy, V. Vaibhav, and D. Srinuvasu, Study of gas turbine exhaust diffuser performance and its enhancement by shape modifications. *ASME Turbo Expo 2010*, Glasgow, UK, 1101–1110 (2010).
5. M. Babu, R. K. Shukla, A. Maru, A. M. Pradeep, and B. Roy, Boundary layer control in turbine exhaust diffusers using casing injection and design modifications. *ASME Turbo Expo 2012*, Copenhagen, Denmark, 1069–1079 (2012).
6. A. Hirschmann, S. Volkmer, M. Casey, and M. Montgomery, Hub extension in an axial gas turbine diffuser. *ASME Turbo Expo 2012*, Copenhagen, Denmark, 1229–1238 (2012).
7. P. Schaefer, W. H. Hofmann, and P. Gieß, Multiobjective optimization for duct and strut design of an annular exhaust diffuser. *ASME Turbo Expo 2012*, Copenhagen, Denmark, 1679–1689 (2012).
8. P. Channaveere and Y. A. Yogananda, Numerical investigation of a divergent exhaust diffuser of a gas turbine engine. International Journal of Innovations in Engineering Research and Technology **4**(6), 31–41 (2017).
9. R. Prakash, D. Christopher, and K. Kumarrathinam, CFD analysis of flow through a conical exhaust diffuser. International Journal of Research in Engineering and Technology **3**(11), 239–248 (2014).
10. B. Salim, Effect of geometrical parameters on the performance of wide angle diffusers. International Journal of Innovative Research in Science Engineering and Technology **2**(9), 4178–4191 (2013).
11. V. Chetan, D. V. Satish, and P. S. Kulkarni, Numerical investigations of PGT10 gas turbine exhaust diffuser using hexahedral dominant grid. International Journal of Engineering and Innovative Technology **3**(1), 392–400 (2013).
12. M. M. Venugopal and V. Somashekar, Design and analysis of annular exhaust diffuser for jet engines. International Journal of Innovative Research in Science Engineering and Technology **4**(7), 5104–5112 (2015).
13. P. Banakar and B. Basawaraj, Computational analysis of flow in afterburner diffuser mixer having different shapes of struts. International Journal of Engineering Research **3**(6), 225–229 (2015).
14. Sakthimurugan, V. and Yuvarajan, D.. A comprehensive assessment on recent advancements in spent fuel reprocessing and waste management: pioneering technologies for a sustainable nuclear future. Kerntechnik (2025).
15. S. Baskar, J. Jayaprabakar, A. Raman, T. Surulivel Rajan, J. Aravind Kumar, U. Nalini

Ramachandran, E. Balaji, P. Sambandam, P.K. Jisha & M. Ruban, Possible bio cathode materials for usage in microbial fuel cells towards energy generation and wastewater treatment to sustain environment: A review, Results in Engineering **25**, 104161 (2025).

16. A. Kumar, B. Rajesh, C. Senthil. Performance study and analysis of Al_2O_3 nanofluid under different flow conditions. *International Journal of Thermal Sciences* **85**, 45–56 (2024).
17. Raja, T., and Y. Devarajan. Thermal evaluation of porcelain filler particles in basalt fibre-reinforced polymer composites for thermal applications. Journal of Thermal Analysis and Calorimetry **149**, 1–13 (2024).